APPLIED MATHEMATICS AND MECHANICS (ENGLISH EDITION)

Extremely large-amplitude oscillation of soft pipes conveying fluid under gravity*

Wei CHEN[1,2],   Ziyang HU[1,2],   Huliang DAI[1,2,†],   Lin WANG[1,2,†]

1. Department of Mechanics, Huazhong University of Science and Technology,
Wuhan 430074, China;

2. Hubei Key Laboratory for Engineering Structural Analysis and Safety Assessment,
Wuhan 430074, China

(Received Mar. 7, 2020 / Revised May 26, 2020)

Abstract   In this work, the nonlinear behaviors of soft cantilevered pipes containing internal fluid flow are studied based on a geometrically exact model, with particular focus on the mechanism of large-amplitude oscillations of the pipe under gravity. Four key parameters, including the flow velocity, the mass ratio, the gravity parameter, and the inclination angle between the pipe length and the gravity direction, are considered to affect the static and dynamic behaviors of the soft pipe. The stability analyses show that, provided that the inclination angle is not equal to π, the soft pipe is stable at a low flow velocity and becomes unstable via flutter once the flow velocity is beyond a critical value. As the inclination angle is equal to π, the pipe experiences, in turn, buckling instability, regaining stability, and flutter instability with the increase in the flow velocity. Interestingly, the stability of the pipe can be either enhanced or weakened by varying the gravity parameter, mainly dependent on the value of the inclination angle. In the nonlinear dynamic analysis, it is demonstrated that the post-flutter amplitude of the soft pipe can be extremely large in the form of limit-cycle oscillations. Besides, the oscillating shapes for various inclination angles are provided to display interesting dynamical behaviors of the inclined soft pipe conveying fluid.

Key words   large-amplitude oscillation, soft pipe conveying fluid, gravity effect, flutter

Chinese Library Classification   O322, O326
2010 Mathematics Subject Classification   37K45, 37K50

1 Introduction

Fluid-structure interactions (FSIs) and flow-induced vibrations (FIVs) commonly exist in practical engineering and have attracted considerable attention from researchers around the world[1–3]. As one of the typical fluid-structure interaction systems, pipes conveying fluid are likely to experience self-excited oscillations[4]. Besides, this FSI pipe system can be found in

---

diverse engineering fields, including the heat exchangers of nuclear reactors, chemical processing plants, oil transportation facilities, and deep-ocean risers. Among various engineering applications, the understanding of the mechanism of fluid-conveying pipes is quite necessary for the purpose of safety designs and precise controls. Furthermore, the dynamical system of pipes conveying fluid is able to show very rich dynamical behaviors, and hence is always chosen as a representative example in various dynamical problems. For these reasons, the literature on the dynamics of pipes conveying fluid has been expanded in the past few decades.

The early works on this topic were mainly concerned with linear vibratory properties, e.g., natural frequencies and vibratory mode, of fluid-conveying pipes[5–9]. Although the self-excited oscillations of a fluid-transporting pipe have already been observed by Brillouin in 1885[10], the first serious study of this problem was conducted by Bourrières in 1939[10] and the basic dynamics was explored by Benjamin[5–6] in 1961. On the basis of extensively experimental and theoretical investigations, the dynamics of cantilevered and supported pipes were found to be fundamentally different. It was demonstrated that both cantilevered and supported pipes will lose stability once the velocity of the internal flow exceeded a critical value[11]. However, the internal-flow-induced instability for a cantilevered pipe is a flutter of vibratory type, while it is a buckling of static type for a supported pipe system[4].

In the subsequent several decades, increasing attention has been devoted to the nonlinear dynamical behaviors of flexible pipes conveying fluid[12–15]. Interestingly, the formulations of supported and cantilevered pipes are also essentially different. For pipes with both ends supported, the curvature of the pipe centerline is relatively small and the nonlinearities are mainly due to the axial extension of the pipe. For cantilevered pipes, however, the pipe centerline is always assumed to be inextensible and the nonlinearities are mostly associated with the curvature of the centerline. In some early works, the governing equations of fluid-conveying pipes were derived ab initio and have different-looking types. In 1994, a new governing equation of cantilevered pipes for planar motions was derived and a definitive comparison was undertaken by Semler et al.[16]. Since then, a large number of studies of cantilevered pipes conveying fluid have been conducted based on the governing equation of Semler et al.[17–19]. It was shown that a plain cantilever conveying fluid would undergo periodic motions when the flow velocity was higher than the critical value. Interestingly, when a cantilevered pipe is modified by adding cubic springs[20–21], tip-end mass[22], and/or motion-limiting constraints[23–24], it is capable of displaying rich dynamical behaviors, including quasiperiodic and chaotic vibrations.

In the governing equation of Semler et al.[16], however, the lateral displacement of the cantilevered pipe was assumed to be relatively small compared with the length of the pipe. For that reason, most subsequent studies on the nonlinear dynamics of a cantilevered pipe conveying fluid were limited to relatively-small-amplitude oscillations. For cantilevered pipes made from very soft materials, however, they may undergo extremely-large-amplitude vibrations. In fact, for a horizontal beam made from soft materials, it may experience large static deformation due to the effect of gravity force[25], and may undergo large-amplitude oscillations in the regime of free vibrations[26]. Naturally, it is of curiosity to understand the large-deformation mechanism of a soft pipe conveying fluid under the gravity effect. To do this, Texier and Dorbolo[27] theoretically predicted and experimentally examined the static deformation of a horizontal pipe conveying fluid by considering the effect of the pipe weight and centrifugal force. Based on the Cosserat rod model, Rivero-Rodriguez and Pérez-Saborid[28] carried out a numerical investigation of the large-amplitude responses of a cantilever conveying fluid in the presence of gravity. However, the numerical procedure given in Ref. [28] may cost a lot of computation time due to the utilization of a Cosserat rod model.

In order to study the extremely-large-amplitude oscillations of fluid-conveying pipes, Chen et al.[29] recently developed a geometrically exact model for planar motions of cantilevered pipes conveying fluid. In their theoretical model, the governing equation of the cantilever was expressed in terms of the rotation angle of the pipe centerline without introducing any approx-

imation of the curvature-dependent nonlinearities. Two types of different-looking governing equations have been derived by Chen et al.[29], and they were demonstrated to be equivalent. Besides, Chen et al.'s geometrically exact equation can be degenerated to the equation derived by Semler et al.[16] with the utilization of a Taylor expansion. However, it must be pointed out that the governing equation of Ref. [29] is limited to the initially vertical pipe and the corresponding static deformation before flutter instability is always zero. The vibrations around zero static configuration of a vertical fluid-conveying pipe are also in a relatively small amplitude range ($\leqslant 0.5$)[29], which are unable to exhibit the extremely large-amplitude oscillations. For an inclined soft pipe conveying fluid, the governing equation given in Ref. [29] is no longer applicable and the static deformations are nonzero. Besides, the dynamical analysis processes of the inclined soft pipe system are more complicated because of the existence of the static large deformation and the potential extremely large-amplitude oscillations.

In this work, with particular attention payed to the dramatic effect of gravity, the nonlinear large-amplitude oscillations of an inclined cantilever conveying fluid are explored. The pipe is assumed to be made from soft materials (e.g., elastomers) with hyper-elastic properties. In the following sections, the governing equation, static deformation, stability analysis, and nonlinear oscillation of the fluid-conveying soft pipe will be presented. The pipe length and gravity directions are generally misaligned, and the inclination angle can significantly affect the behaviors of the pipe due to the gravity effect. In this way, large deformations of the pipe would occur, and the theoretical model based on the relatively small-amplitude vibration theory will no longer be valid. Compared with the Cosserat rod model of Ref. [28], the proposed model is described in a much simpler form since only one displacement variable is contained in the governing equation.

2 Analytical model and formulation

2.1 Analytical model

As shown in Fig. 1, the system under consideration consists of a soft pipe of length L, cross-sectional area A, inertia moment I, elastic modulus E, mass per unit length m, and conveying fluid of mass per unit length M with flow velocity U. The pipe is initially straight, and its inclined angle is α with respect to the vertical direction. The considered pipe is slender,
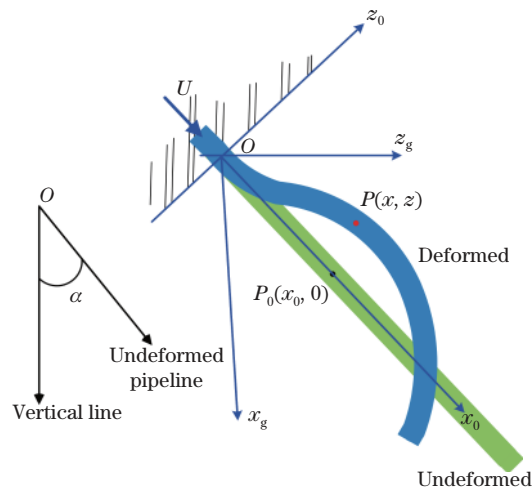

Fig. 1 Schematic diagram of a cantilevered soft pipe conveying fluid under gravity and undeformed and deformed shapes (color online)

and hence the Euler-Bernoulli beam theory is reliable for this problem. The geometric nonlinearity of the pipe will be exactly accounted for so as to capture the large and extremely large deformations of the pipe. For this purpose, the cantilevered pipe is assumed to be inextensible according to the discussion by Ghayesh et al.[30]. Thus, the strain of the soft pipe is small, and the linear elastic constitutive relation is still available. The considered fluid is incompressible with a plug-flow assumption, and the motion of the pipe is assumed to be planar.

In order to derive the governing equation of the pipe system, two sets of coordinate systems, i.e., the local coordinate system (x_0, z_0) and the global coordinate system (x_g, z_g), are introduced. In the local coordinate system, the x_0-axis is along the centerline of the undeformed pipe, and the positions of the pipe centerline are, respectively, denoted as $(x_0, 0)$ and (x, z) for the undeformed and deformed pipes. In the global coordinate system, the x_g-axis is along the direction of gravity (i.e., the vertical line), and the position of the pipe centerline is denoted as (x_g, z_g). In the following formulation, the motion of the pipe is described in the frame of the local coordinate system.

2.2 Governing equation

The displacement vector of the pipe centerline is the subtraction of the coordinates in the current (deformed) and reference (undeformed) configurations. It can be expressed as

$$\boldsymbol{d} = (u, w) = (x - x_0, z), \tag{1}$$

where $u = u(x_0, t)$ is the axial displacement and $w = w(x_0, t)$ is the lateral displacement. Besides, the unit vector in the opposite direction of gravity is given by

$$\boldsymbol{n}_v = (-\cos\alpha, \sin\alpha). \tag{2}$$

For an inextensible pipe, the relationships between the displacements u and w and the rotation angle θ of the centerline are given by[31]

$$\frac{\partial u}{\partial x_0} = \cos\theta - 1, \quad \frac{\partial w}{\partial x_0} = \sin\theta. \tag{3}$$

In this work, the considered boundary conditions of the pipe are clamped-free. Therefore, we have

$$u(0, t) = 0, \quad w(0, t) = 0. \tag{4}$$

By utilizing the boundary conditions of Eq. (4), the axial and lateral displacements can be written as

$$u = \int_0^{x_0} \cos\theta \mathrm{d}x_0 - x_0, \quad w = \int_0^{x_0} \sin\theta \mathrm{d}x_0. \tag{5}$$

The velocity vector of the pipe element is

$$\boldsymbol{V}_{\mathrm{p}} = \Big(\frac{\partial x}{\partial t}, \frac{\partial z}{\partial t}\Big). \tag{6}$$

However, the velocity vector of the fluid element is more complicated. It is given by[16]

$$\boldsymbol{V}_{\mathrm{f}} = \frac{\partial}{\partial t}(x\boldsymbol{i} + z\boldsymbol{k}) + U\frac{\partial}{\partial s}(x\boldsymbol{i} + z\boldsymbol{k}). \tag{7}$$

According to the inextensible assumption, we have $\mathrm{d}s = \mathrm{d}x_0$, where $\mathrm{d}s$ is the element length after deformation. Therefore, the total kinetic energy of the system can be expressed as[16]

$$T = \frac{1}{2}m\int_0^L \Big(\Big(\frac{\partial x}{\partial t}\Big)^2 + \Big(\frac{\partial z}{\partial t}\Big)^2\Big)\mathrm{d}x_0 + \frac{1}{2}M\int_0^L \Big(\Big(\frac{\partial x}{\partial t} + U\frac{\partial x}{\partial x_0}\Big)^2 + \Big(\frac{\partial z}{\partial t} + U\frac{\partial z}{\partial x_0}\Big)^2\Big)\mathrm{d}x_0. \tag{8}$$

With the help of Eqs. (1), (3), and (5), the variation of Eq. (8) leads to

$$\delta \int_{t_1}^{t_2} T \mathrm{d}t = \int_{t_1}^{t_2} \int_0^L \left(\int_{x_0}^L \left((m+M)\frac{\partial^2 u}{\partial t^2} + M\frac{\partial U}{\partial t}\left(\frac{\partial u}{\partial x_0} + 1\right) + 2MU\frac{\partial^2 u}{\partial x_0 \partial t} \right) \mathrm{d}x_0 \right) \sin\theta \delta\theta \mathrm{d}x_0 \mathrm{d}t$$

$$- \int_{t_1}^{t_2} \int_0^L \left(\int_{x_0}^L \left((m+M)\frac{\partial^2 w}{\partial t^2} + M\frac{\partial U}{\partial t}\frac{\partial w}{\partial x_0} + 2MU\frac{\partial^2 w}{\partial x_0 \partial t} \right) \mathrm{d}x_0 \right) \cos\theta \delta\theta \mathrm{d}x_0 \mathrm{d}t$$

$$+ MU \int_{t_1}^{t_2} \left(\frac{\partial x_L}{\partial t}\delta x_L + \frac{\partial z_L}{\partial t}\delta z_L \right) \mathrm{d}t, \tag{9}$$

where the subscript L denotes the value at $x_0 = L$. Based on the nonlinear Euler-Bernoulli beam theory, the variation of the strain energy of an inextensible pipe is[29]

$$\delta \int_{t_1}^{t_2} \mathcal{V}\mathrm{d}t = \delta\left(\int_{t_1}^{t_2} \int_0^L \frac{1}{2}EI\left(\frac{\partial\theta}{\partial x_0}\right)^2 \mathrm{d}x_0 \mathrm{d}t \right)$$

$$= EI \int_{t_1}^{t_2} \frac{\partial\theta}{\partial x_0}\delta\theta \Big|_0^L \mathrm{d}t - EI \int_{t_1}^{t_2} \int_0^L \frac{\partial^2\theta}{\partial x_0^2}\delta\theta \mathrm{d}x_0 \mathrm{d}t. \tag{10}$$

It can be seen from Eq. (10) that, the curvature of the pipe centerline is exactly considered without any approximation. This enables the investigation of large and extremely large deformations of the pipe. The variation of the gravitational potential of the system is

$$\delta \int_{t_1}^{t_2} \mathcal{G}\mathrm{d}t = (m+M)g \int_{t_1}^{t_2} \int_0^L \delta(\boldsymbol{d}\cdot\boldsymbol{n}_v)\mathrm{d}x_0 \mathrm{d}t$$

$$= (m+M)g \int_{t_1}^{t_2} \int_0^L (-\cos\alpha\delta u + \sin\alpha\delta w)\mathrm{d}x_0 \mathrm{d}t$$

$$= \int_{t_1}^{t_2} \left(\int_0^L (m+M)g(L-x_0)\sin(\theta+\alpha)\delta\theta\mathrm{d}x_0 \right)\mathrm{d}t. \tag{11}$$

In addition, the cantilevered pipe conveying fluid is one type of open systems, Hamilton's principle for this non-conservative system is[5,16]

$$\delta \int_{t_1}^{t_2} \mathcal{L}\mathrm{d}t = \int_{t_1}^{t_2} \left(MU\left(\frac{\partial\boldsymbol{r}_L}{\partial t} + U\boldsymbol{\tau}_L\right)\cdot\delta\boldsymbol{r}_L \right)\mathrm{d}t, \tag{12}$$

where $\mathcal{L}$ is the Lagrangian of the pipe system $(\mathcal{L} = T - \mathcal{V} - \mathcal{G})$, $\boldsymbol{r}$ is the position vector (x, z), and $\boldsymbol{\tau}$ is the unit vector tangential to the pipe centerline $\left(\frac{\partial x}{\partial x_0}, \frac{\partial z}{\partial x_0}\right)$. Furthermore, the right-hand side in Eq. (12) can be rewritten as

$$E_{\mathrm{rhs}} = MU \int_{t_1}^{t_2} \left(\frac{\partial x_L}{\partial t}\delta x_L + \frac{\partial z_L}{\partial t}\delta z_L \right)\mathrm{d}t + MU^2 \int_{t_1}^{t_2} \left(\frac{\partial x_L}{\partial x_0}\delta x_L + \frac{\partial z_L}{\partial x_0}\delta z_L \right)\mathrm{d}t. \tag{13}$$

Automatically, the first term in Eq. (13) cancels the last term in Eq. (9). The second term in Eq. (13) can be further rewritten as

$$MU^2 \int_{t_1}^{t_2} \left(\frac{\partial x_L}{\partial t}\delta x_L + \frac{\partial z_L}{\partial t}\delta z_L \right)\mathrm{d}t = MU^2 \int_{t_1}^{t_2} \int_0^L \sin(\theta_L - \theta)\delta\theta\mathrm{d}x_0 \mathrm{d}t. \tag{14}$$

Combining Eqs. (9), (10), (11), (13), and (14) into Eq. (12), one obtains the governing equation

$$\left(\int_{x_0}^{L} \left((m+M)\int_0^{x_0} \left(\frac{\partial^2\theta}{\partial t^2}\sin\theta + \left(\frac{\partial\theta}{\partial t}\right)^2\cos\theta\right)\mathrm{d}x_0 - M\frac{\partial U}{\partial t}\cos\theta + 2MU\frac{\partial\theta}{\partial t}\sin\theta\right)\mathrm{d}x_0\right)\sin\theta$$

$$+\left(\int_{x_0}^{L} \left((m+M)\int_0^{x_0} \left(\frac{\partial^2\theta}{\partial t^2}\cos\theta - \left(\frac{\partial\theta}{\partial t}\right)^2\sin\theta\right)\mathrm{d}x_0 + M\frac{\partial U}{\partial t}\sin\theta + 2MU\frac{\partial\theta}{\partial t}\cos\theta\right)\mathrm{d}x_0\right)\cos\theta$$

$$- EI\frac{\partial^2\theta}{\partial x_0^2} + (m+M)g(L-x_0)\sin(\theta+\alpha) + MU^2\sin(\theta_L - \theta) = 0 \tag{15}$$

and the boundary conditions

$$\theta = 0 \quad \text{or} \quad \theta' = 0 \quad \text{at} \quad x_0 = 0 \quad \text{and} \quad x_0 = L. \tag{16}$$

For the purpose of completing the governing equation, the dissipative term due to the viscoelasticity of the soft pipe needs to be added. The Kelvin-Voigt model suggests the following constitutive relation[32]:

$$\sigma = E\varepsilon + E^*\frac{\partial\varepsilon}{\partial t}, \tag{17}$$

in which σ is the stress, and ε is the strain. According to the approach given by Stoker[31], the strain energy may be modified by

$$E \to E\left(1 + a\left(\frac{\partial}{\partial t}\right)\right). \tag{18}$$

Hence, the viscoelasticity of the soft pipe can be considered by replacing the term $-EI\theta$ by $-E(1 + a(\frac{\partial}{\partial t}))I\theta$ in Eq. (15).

2.3 Nondimensionalization of the governing equation

In order to reduce the number of system parameters and simplify the form of the governing equation, the following dimensionless quantities are introduced:

$$\begin{cases} \xi = \dfrac{x_0}{L}, \quad \varsigma = \dfrac{u}{L}, \quad \eta = \dfrac{w}{L}, \quad \tau = \left(\dfrac{EI}{m+M}\right)^{1/2}\dfrac{t}{L^2}, \\[2mm] \mu = \left(\dfrac{EI}{m+M}\right)^{1/2}\dfrac{a}{L^2}, \quad v = \left(\dfrac{M}{EI}\right)^{1/2}UL, \quad \gamma = \dfrac{m+M}{EI}L^3g, \quad \beta = \dfrac{M}{m+M}, \end{cases} \tag{19}$$

where γ is the gravity parameter, and β is the mass ratio. Substituting Eq. (19) into the modified governing equation, one obtains

$$\sin\theta \int_\xi^1 \int_0^\xi \left(\frac{\partial^2\theta}{\partial\tau^2}\sin\theta + \left(\frac{\partial\theta}{\partial\tau}\right)^2\cos\theta\right)\mathrm{d}\xi\mathrm{d}\xi$$

$$+ \sin\theta \int_\xi^1 \left(-\frac{\partial v}{\partial\tau}\sqrt{\beta}\cos\theta + 2v\sqrt{\beta}\frac{\partial\theta}{\partial\tau}\sin\theta\right)\mathrm{d}\xi$$

$$+ \cos\theta \int_\xi^1 \int_0^\xi \left(\frac{\partial^2\theta}{\partial\tau^2}\cos\theta - \left(\frac{\partial\theta}{\partial\tau}\right)^2\sin\theta\right)\mathrm{d}\xi\mathrm{d}\xi$$

$$+ \cos\theta \int_\xi^1 \left(\frac{\partial v}{\partial\tau}\sqrt{\beta}\sin\theta + 2v\sqrt{\beta}\frac{\partial\theta}{\partial\tau}\cos\theta\right)\mathrm{d}\xi$$

$$- \frac{\partial^2\theta}{\partial\xi^2} - \mu\frac{\partial^3\theta}{\partial\xi^2\partial\tau} + \gamma(1-\xi)\sin(\theta+\alpha) + v^2\sin(\theta_1-\theta) = 0. \tag{20}$$

For a cantilevered pipe, the boundary conditions for the rotation angle θ are given by

$$\theta(0, \tau) = 0, \quad \frac{\partial \theta(1, \tau)}{\partial \xi} = 0. \tag{21}$$

Obviously, a closed-form solution of Eq. (20) is not available. Consequently, numerical solutions will be given in Sections 3 and 4.

2.4   Galerkin discretization

In this subsection, the partial differential equation (20) with an infinite dimension will be discretized into a set of nonlinear ordinary equations. According to Galerkin's technique, the rotation angle $\theta(\xi, \tau)$ can be approximated by the following series expansion:

$$\theta(\xi, \tau) = \sum_{r=1}^{N} \phi_r(\xi) q_r(\tau), \tag{22}$$

where $\phi_r(\xi)$ are the base functions that satisfy the boundary conditions (21) with the specific expression of

$$\phi_r(\xi) = \sin\left(\frac{2r-1}{2}\pi\xi\right),$$

$q_r(\tau)$ are the corresponding generalized coordinates, and N is the number of truncated modes. The substitution of Eq. (22) into Eq. (20), followed by multiplication by $\phi_i(\xi)$ and integration from 0 to 1, yields

$$\boldsymbol{M}\left(\frac{\mathrm{d}^2\boldsymbol{q}}{\mathrm{d}\tau^2}\right) + \boldsymbol{C}\left(\frac{\mathrm{d}\boldsymbol{q}}{\mathrm{d}\tau}\right) + \boldsymbol{K}(\boldsymbol{q}) + \left(\mathcal{N}_1(\boldsymbol{q})\right) + \left(\mathcal{N}_2\left(\boldsymbol{q}, \frac{\mathrm{d}\boldsymbol{q}}{\mathrm{d}\tau}\right)\right) = 0, \tag{23}$$

where

$$M_{ij} = \int_0^1 \phi_i\left(\sin\left(\sum_{m=1}^{N}\phi_m q_m\right)\int_\xi^1 \int_0^\xi \phi_j \sin\left(\sum_{m=1}^{N}\phi_m q_m\right)\mathrm{d}\xi\mathrm{d}\xi\right)\mathrm{d}\xi$$
$$+ \int_0^1 \phi_i\left(\cos\left(\sum_{m=1}^{N}\phi_m q_m\right)\int_\xi^1 \int_0^\xi \phi_j \cos\left(\sum_{m=1}^{N}\phi_m q_m\right)\mathrm{d}\xi\mathrm{d}\xi\right)\mathrm{d}\xi, \tag{24a}$$

$$C_{ij} = -\mu \int_0^1 \phi_i \phi_j'' \mathrm{d}\xi, \tag{24b}$$

$$K_{ij} = -\int_0^1 \phi_i \phi_j'' \mathrm{d}\xi, \tag{24c}$$

$$\mathcal{N}_{1i} = \gamma\left(\int_0^1 \phi_i\left(1 - \xi\right)\sin\left(\sum_{j=1}^{N}\phi_j q_j + \alpha\right)\mathrm{d}\xi\right)$$
$$+ v^2\left(\int_0^1 \phi_i \sin\left(\left(\sum_{j=1}^{N}\phi_j(1)q_j\right) - \left(\sum_{j=1}^{N}\phi_j q_j\right)\right)\mathrm{d}\xi\right)$$
$$- \frac{\partial v}{\partial \tau}\sqrt{\beta}\left(\int_0^1 \phi_i \sin\left(\sum_{m=1}^{N}\phi_m q_m\right)\left(\int_\xi^1 \cos\left(\sum_{m=1}^{N}\phi_m q_m\right)\mathrm{d}\xi\right)\mathrm{d}\xi\right)$$
$$+ \frac{\partial v}{\partial \tau}\sqrt{\beta}\left(\int_0^1 \phi_i \cos\left(\sum_{m=1}^{N}\phi_m q_m\right)\left(\int_\xi^1 \sin\left(\sum_{m=1}^{N}\phi_m q_m\right)\mathrm{d}\xi\right)\mathrm{d}\xi\right), \tag{24d}$$

$$\mathcal{N}_{2i} = \int_0^1 \phi_i \Big(\sin \Big(\sum_{m=1}^N \phi_m q_m \Big) \Big(\int_\xi^1 \int_0^\xi \Big(\phi_j \frac{\mathrm{d}q_j}{\mathrm{d}\tau} \Big)^2 \cos \Big(\sum_{m=1}^N \phi_m q_m \Big) \mathrm{d}\xi \mathrm{d}\xi \Big) \Big) \mathrm{d}\xi$$

$$+ 2v\sqrt{\beta} \Big(\int_0^1 \phi_i \sin \Big(\sum_{m=1}^N \phi_m q_m \Big) \Big(\int_\xi^1 \Big(\phi_j \frac{\mathrm{d}q_j}{\mathrm{d}\tau} \Big) \sin \Big(\sum_{m=1}^N \phi_m q_m \Big) \mathrm{d}\xi \Big) \mathrm{d}\xi \Big)$$

$$- \Big(\int_0^1 \phi_i \cos \Big(\sum_{m=1}^N \phi_m q_m \Big) \Big(\int_\xi^1 \int_0^\xi \Big(\phi_j \frac{\mathrm{d}q_j}{\mathrm{d}\tau} \Big)^2 \sin \Big(\sum_{m=1}^N \phi_m q_m \Big) \mathrm{d}\xi \mathrm{d}\xi \Big) \mathrm{d}\xi \Big)$$

$$+ 2v\sqrt{\beta} \Big(\int_0^1 \phi_i \cos \Big(\sum_{m=1}^N \phi_m q_m \Big) \Big(\int_\xi^1 \Big(\phi_j \frac{\mathrm{d}q_j}{\mathrm{d}\tau} \Big) \cos \Big(\sum_{m=1}^N \phi_m q_m \Big) \mathrm{d}\xi \Big) \mathrm{d}\xi \Big). \qquad (24\mathrm{e})$$

In order to implement numerical simulations, the discretized equation (23) is reduced to the first-order form by introducing $\boldsymbol{p} = \mathrm{d}\boldsymbol{q}/\mathrm{d}\tau$. Therefore, one obtains

$$\begin{pmatrix} \dfrac{\mathrm{d}\boldsymbol{q}}{\mathrm{d}\tau} \\[2mm] \dfrac{\mathrm{d}\boldsymbol{p}}{\mathrm{d}\tau} \end{pmatrix} = \begin{pmatrix} \boldsymbol{0} & \boldsymbol{I} \\ -\boldsymbol{M}^{-1}\boldsymbol{K} & -\boldsymbol{M}^{-1}\boldsymbol{C} \end{pmatrix} \begin{pmatrix} \boldsymbol{q} \\ \boldsymbol{p} \end{pmatrix} + \begin{pmatrix} \boldsymbol{0} \\ -\boldsymbol{M}^{-1}\mathcal{N}_1(\boldsymbol{q}) - \boldsymbol{M}^{-1}\mathcal{N}_2(\boldsymbol{q},\boldsymbol{p}) \end{pmatrix}. \qquad (25)$$

In what follows, Eq. (25) will be solved by a fourth-order Runge-Kutta integration algorithm with variable time steps. Besides, the velocity of the rotation angle is given by

$$\frac{\partial \theta}{\partial \tau} = \sum_{r=1}^N \phi_r(\xi) p_r(\tau). \qquad (26)$$

With the aid of Eqs. (22) and (26), the oscillation velocities of the pipe can be given by

$$\begin{cases} \dfrac{\partial \zeta}{\partial \tau} = -\displaystyle\int_0^\xi \sum_{m=1}^N \phi_m(\xi) p_m(\tau) \sin \Big(\sum_{m=1}^N \phi_m(\xi) q_m(\tau) \Big) \mathrm{d}\xi, \\[4mm] \dfrac{\partial \eta}{\partial \tau} = \displaystyle\int_0^\xi \sum_{m=1}^N \phi_m(\xi) p_m(\tau) \cos \Big(\sum_{m=1}^N \phi_m(\xi) q_m(\tau) \Big) \mathrm{d}\xi. \end{cases} \qquad (27)$$

Furthermore, the dimensionless coordinates $(X_\mathrm{g}, Z_\mathrm{g})$ of the deformed pipe centerline in the global coordinate system are

$$X_\mathrm{g} = \int_0^\xi \cos \Big(\sum_{m=1}^N \phi_m(\xi) q_m(\tau) + \alpha \Big) \mathrm{d}\xi, \quad Z_\mathrm{g} = \int_0^\xi \sin \Big(\sum_{m=1}^N \phi_m(\xi) q_m(\tau) + \alpha \Big) \mathrm{d}\xi. \qquad (28)$$

According to Eq. (28), the deformed configuration of the pipe can be determined.

3   Static deformation

3.1   Convergence test and validation of the analytical model

To check the numerical scheme, the static deformation of a soft pipe conveying fluid with different inclination angles α will be studied in this section. It should be pointed out that the determination of the static deformation is very important for the later stability analyses of the pipe system, which will be seen in Section 4.

Before doing extensive calculations, the verification of a suitable number N of truncated modes is necessary. By dropping the dynamic terms in Eq. (20), it is found that the static deformations of the pipe are mainly associated with three system parameters, including the

dimensionless flow velocity v, the gravity parameter γ, and the inclination angle α. First, the gravity parameter $\gamma = 18.9$, which is coincident with the experimental data of a silicone rubber pipe conveying water obtained by Païdoussis and Semler[33], will be adopted in the convergence test. As shown in Fig. 2(a), $N = 3$ is valid in the calculations of the static deformations of the pipe.

Next, the theoretical and experimental results obtained by Texier and Dorbolo[27] will be used for comparison. The pipe system with $L = 94\,\text{mm}$, $EI = 1.8 \times 10^{-5}\,\text{N·m}^2$, $m = 15.9\,\text{g/m}$, $M = 5.8\,\text{g/m}$, and $\alpha = \pi/2$ is considered. The corresponding dimensionless quantities are found to be

$$\beta = \frac{M}{M+m} = \frac{5.8}{5.8+15.9} = 0.267\,3, \tag{29a}$$

$$\gamma = \frac{m+M}{EI}L^3 g = \frac{21.7\,(\text{g/m})}{1.8 \times 10^{-5}\,(\text{N} \cdot \text{m}^2)} \times 0.094^3\,(\text{m}^3) \times 9.8\,(\text{N/kg}) = 9.812\,9, \tag{29b}$$

$$v = \left(\frac{M}{EI}\right)^{1/2} UL = \sqrt{\frac{5.8\,(\text{g/m})}{1.8 \times 10^{-5}\,(\text{N} \cdot \text{m}^2)}} \times 0.094\,\text{m} \times \overline{U}\,(\text{m/s}) = 1.687\,4\overline{U}, \tag{29c}$$

where $\overline{U}$ is the dimensional value of the flow velocity. It can be seen from Fig. 2(b) that, our results agree well with the previous theoretical result and experimental data given in Ref. [27]. Furthermore, Fig. 2 indicates that when $v = 0$, the pipe experiences the largest static deformation due to the gravity force. As the flow velocity is increased, the pipe shape will gradually return to its initially undeformed one. According to Eq. (20), when the flow velocity is sufficiently high, the soft pipe will tend to straighten. However, in most cases, the cantilevered soft pipe is impossible to recover the undeformed straight shape. When the flow velocity reaches a critical value, indeed, the dynamic (time-dependent) terms in the governing equation will take effects and flutter instability may occur, generating oscillations of the pipe.
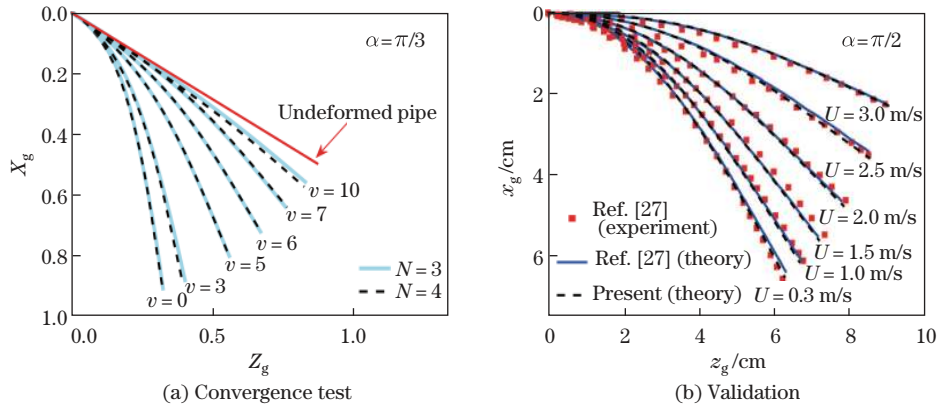

Fig. 2   Convergence test and validation of the deformed configuration of the pipe (color online)

3.2   Effects of the gravity parameter γ

In order to investigate the effects of the gravity parameter on the static deformation of the pipe, the current configurations for $\gamma = 10$, 30, and 100 are shown in Fig. 3 for various values of the flow velocity. It can be observed that the deformation of the pipe becomes larger as the gravity parameter is increased. This is not surprising since more gravitational potential energy is contained in the pipe system when γ increases. Furthermore, according to Eq. (20), when γ is sufficiently large, the solution of the static deformation of the pipe is $\theta \approx -\alpha$, which implies that the deformed pipe is shaped as a plumb line.
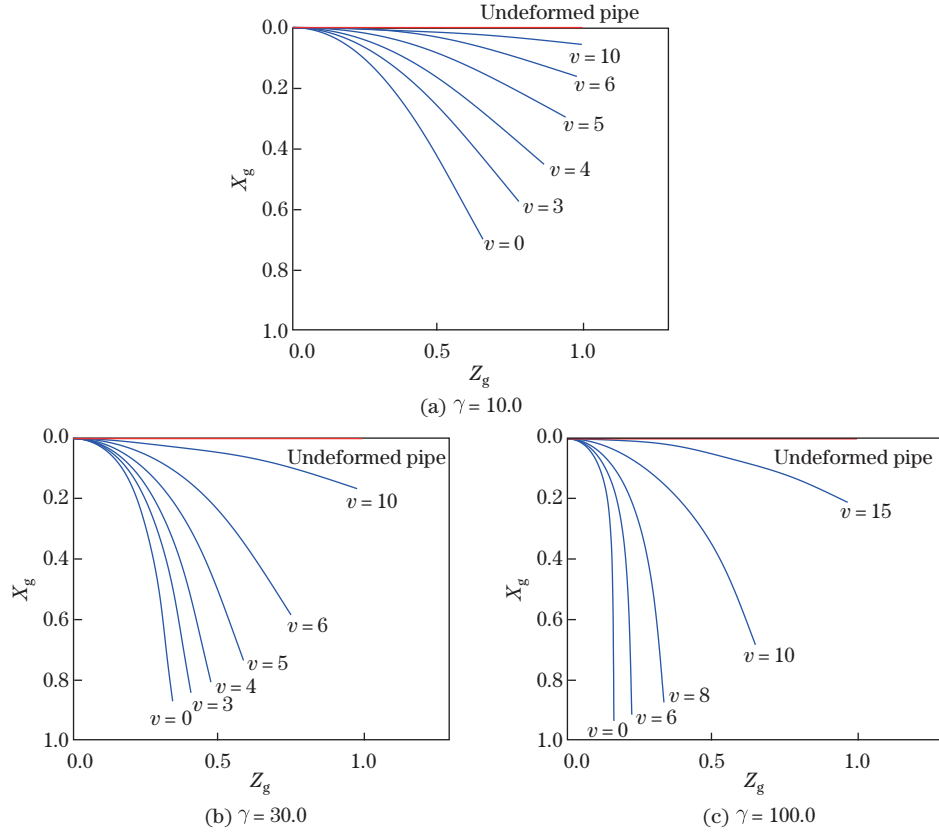
Fig. 3 Current configurations of the pipe ($\alpha = \pi/2$) with different values of γ for various flow velocities (color online)

3.3 Effects of the inclination angle α

The effects of the inclination angle α on the static deformation of the pipe can be seen in Figs. 2(a) and 4. In these figures, the results for $\alpha = \pi/3$, $\pi/2$, $3\pi/4$, and $9\pi/10$ are given. As shown, the inclination angle has a significant effect on the static deformation of the pipe. Bearing in mind that the static deformation of the pipe is strongly dependent on the gravity force, it is natural to understand that the dependence of the static deformation of the pipe on α is essentially due to the presence of the gravity force.

4 Stability analyses

As mentioned in Subsection 3.1, the static deformation results are only available when the pipe is stable. When the flow velocity reaches a critical value, the dynamic terms in Eq. (20) become important, and the pipe is possible to undergo dynamical instability. For the purpose of further studying the responses of the pipe system, the stability analyses will be conducted in what follows.

To determine the stability of the system about the static deformation of the pipe, the rotation angle $\theta(\xi, \tau)$ is separated into two parts, i.e.,

$$\theta(\xi, \tau) = \theta^{\mathrm{s}}(\xi) + \theta^{\mathrm{d}}(\xi, \tau), \tag{30}$$

where $\theta^{\mathrm{s}}(\xi)$ is the steady (static) part of the rotation angle, and $\theta^{\mathrm{d}}(\xi, \tau)$ is the dynamical part (perturbation) about the steady part. The substitution of Eq. (30) into the dimensionless
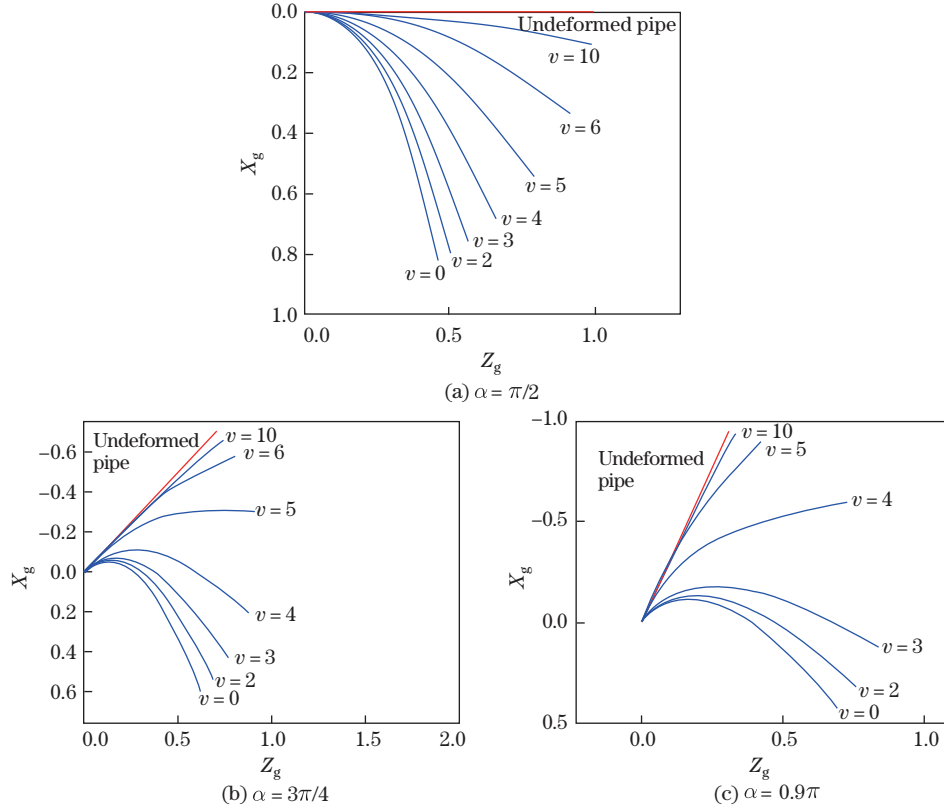
Fig. 4 Current configurations of the pipe ($\gamma = 18.9$) for different values of α with various flow velocities (color online)

governing equation (20), followed by Taylor expanding the nonlinear terms about $\theta^{\mathrm{d}} = 0$ and keeping the linear terms of $\theta^{\mathrm{d}}(\xi, \tau)$ yields the governing equations for the static equilibrium and dynamical behavior of the pipe system about the static equilibrium as follows:

$$-\frac{\partial^2 \theta^{\mathrm{s}}}{\partial \xi^2} + \gamma(1 - \xi)\sin(\theta^{\mathrm{s}} + \alpha) + v^2 \sin(\theta_1^{\mathrm{s}} - \theta^{\mathrm{s}}) = 0, \tag{31a}$$

$$\sin\theta^{\mathrm{s}} \int_\xi^1 \int_0^\xi \left(\sin\theta^{\mathrm{s}}\frac{\partial^2\theta^{\mathrm{d}}}{\partial\tau^2}\right)\mathrm{d}\xi\mathrm{d}\xi + \sin\theta^{\mathrm{s}} \int_\xi^1 \left(2v\sqrt{\beta}\sin\theta^{\mathrm{s}}\frac{\partial\theta^{\mathrm{d}}}{\partial\tau}\right)\mathrm{d}\xi$$

$$+ \cos\theta^{\mathrm{s}} \int_\xi^1 \int_0^\xi \left(\cos\theta^{\mathrm{s}}\frac{\partial^2\theta^{\mathrm{d}}}{\partial\tau^2}\right)\mathrm{d}\xi\mathrm{d}\xi + \cos\theta^{\mathrm{s}} \int_\xi^1 \left(2v\sqrt{\beta}\cos\theta^{\mathrm{s}}\frac{\partial\theta^{\mathrm{d}}}{\partial\tau}\right)\mathrm{d}\xi$$

$$-\frac{\partial^2\theta^{\mathrm{d}}}{\partial\xi^2} - \mu\frac{\partial^3\theta^{\mathrm{d}}}{\partial\xi^2\partial\tau} + \gamma(1 - \xi)\cos(\theta^{\mathrm{s}} + \alpha)\theta^{\mathrm{d}} + v^2(\theta_1^{\mathrm{d}} - \theta^{\mathrm{d}})\cos(\theta_1^{\mathrm{s}} - \theta^{\mathrm{s}}) = 0. \tag{31b}$$

The solution of Eq. (31a) has already been discussed in Section 3. Based on the static deformation results, we can carry out the stability analyses with the aid of the Galerkin method. An analogous process of Subsection 2.4 leads to the discretized form of Eq. (31b) as follows:

$$\boldsymbol{M}^{\mathrm{d}}\frac{\mathrm{d}^2\boldsymbol{q}^{\mathrm{d}}}{\mathrm{d}\tau^2} + \boldsymbol{C}^{\mathrm{d}}\frac{\mathrm{d}\boldsymbol{q}^{\mathrm{d}}}{\mathrm{d}\tau} + \boldsymbol{K}^{\mathrm{d}}\boldsymbol{q}^{\mathrm{d}} = \boldsymbol{0}, \tag{32}$$

where

$$M_{ij}^{\mathrm{d}} = \int_0^1 \left(\phi_i \sin\theta^{\mathrm{s}} \int_\xi^1 \int_0^\xi \phi_j \sin\theta^{\mathrm{s}} \mathrm{d}\xi\mathrm{d}\xi \right)\mathrm{d}\xi + \int_0^1 \left(\phi_i \cos\theta^{\mathrm{s}} \int_\xi^1 \int_0^\xi \phi_j \cos\theta^{\mathrm{s}}\mathrm{d}\xi\mathrm{d}\xi \right)\mathrm{d}\xi, \quad (33\mathrm{a})$$

$$C_{ij}^{\mathrm{d}} = 2v\sqrt{\beta} \int_0^1 \left(\phi_i \sin\theta^{\mathrm{s}} \int_\xi^1 \phi_j \sin\theta^{\mathrm{s}}\mathrm{d}\xi \right)\mathrm{d}\xi + 2v\sqrt{\beta} \int_0^1 \left(\phi_i \cos\theta^{\mathrm{s}} \int_\xi^1 \phi_j \cos\theta^{\mathrm{s}}\mathrm{d}\xi \right)\mathrm{d}\xi$$

$$- \mu \int_0^1 \phi_i \phi_j''\mathrm{d}\xi, \qquad (33\mathrm{b})$$

$$K_{ij}^{\mathrm{d}} = -\int_0^1 \phi_i \phi_j''\mathrm{d}\xi + \gamma \int_0^1 ((1-\xi)\phi_i \cos(\theta^{\mathrm{s}} + \alpha)\phi_j)\mathrm{d}\xi$$

$$+ v^2 \int_0^1 \phi_i(\phi_j(1) - \phi_j)\cos(\theta_1^{\mathrm{s}} - \theta^{\mathrm{s}})\mathrm{d}\xi, \qquad (33\mathrm{c})$$

$$\theta^{\mathrm{d}}(\xi,\tau) = \sum_{r=1}^N \phi_r(\xi)q_r^{\mathrm{d}}(\tau). \qquad (33\mathrm{d})$$

After reducing Eq. (32) to its first-order form by introducing $\boldsymbol{p}^{\mathrm{d}} = \mathrm{d}\boldsymbol{q}^{\mathrm{d}}/(\mathrm{d}\tau)$, the stability of the FSI system can be determined by solving the eigenvalue problem. The typical results are shown in Figs. 5 and 6.
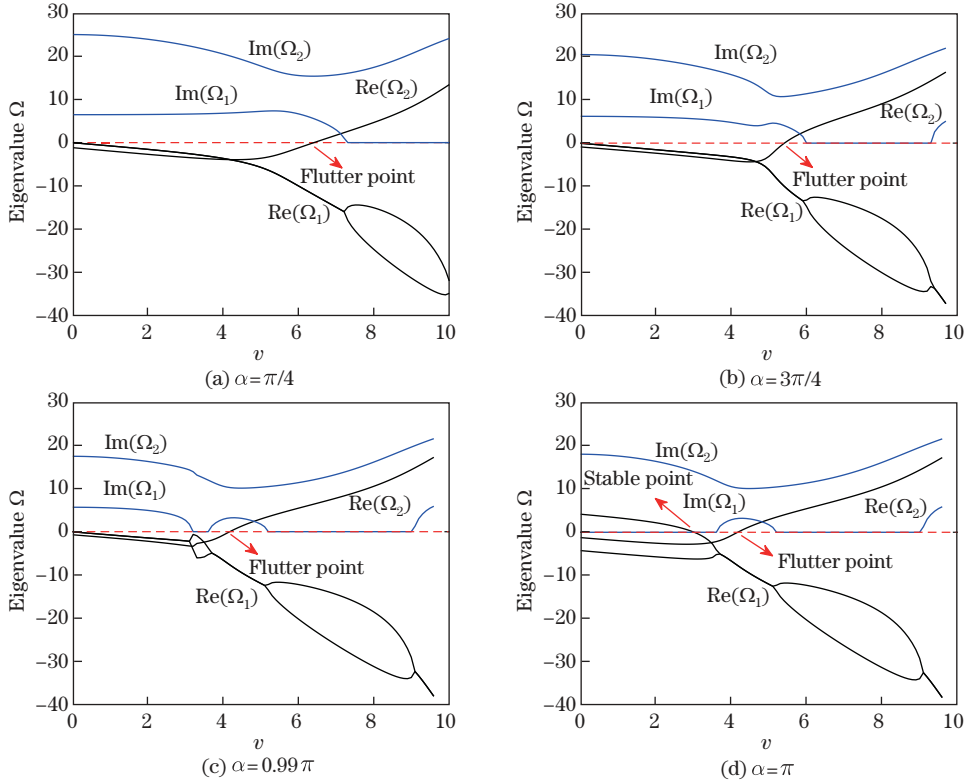

Fig. 5 Eigenvalue Ω of the pipe system for different values of α, when $\beta = 0.142$, $\gamma = 18.9$, and $\mu = 5 \times 10^{-3}$, with various values of the flow velocity (color online)

(a) Different values of mass ratio with $\gamma = 18.9$ (b) Different values of gravity parameter with $\beta = 0.142$
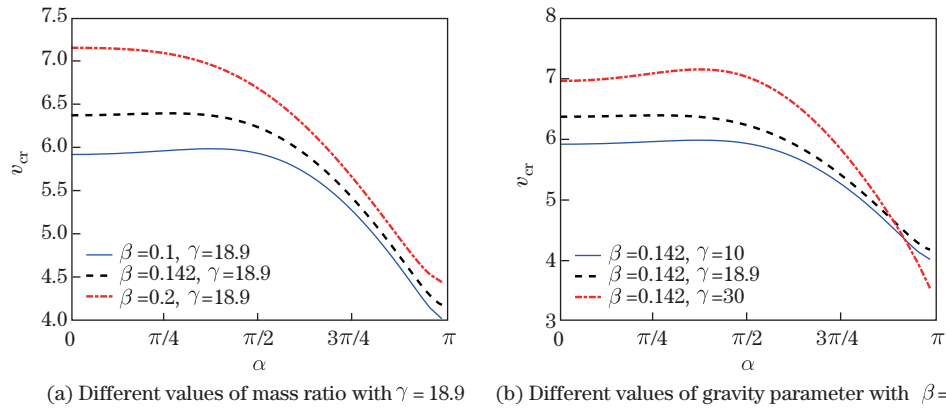
Fig. 6 Evolution of the critical flow velocities for flutter with increasing α (color online)

During the calculations of Fig. 5 (and all later results in Section 5), several key system parameters are chosen as the same as those utilized by Païdoussis and Semler[33], i.e.,

$$\beta = 0.142, \quad \gamma = 18.9, \quad \mu = 5 \times 10^{-3}.$$

These values of system parameters are for an elastomer (silicone rubber) pipe devised in Ref. [33]. The stability analyses show that there is a critical flow velocity v_{cr} for flutter when $\alpha \neq \pi$. The pipe is stable with a static deformation when the flow velocity is smaller than the critical value. As can be seen in Figs. 5(a), 5(b), and 5(c), the pipe will lose stability via flutter in the second mode. In the case of $\alpha = \pi$, however, with the gradual increase in the flow velocity, the pipe will, sequentially, be subjected to buckling instability in the first mode, become stable, and lose stability via flutter in the second mode, as shown in Fig. 5(d).

The critical flow velocities for different system parameters are shown in Fig. 6. It should be mentioned that all stability results have been verified to be convergent for the Galerkin discretization. It is obvious that the stability of the pipe system is weakened with increasing the inclination angle. This is reasonable since the potential energy of the system increases while the stiffness decreases when α is increased. As the mass ratio is increased, the stability of the pipe system is enhanced. This can be expected since the mass of the pipe system is added. However, when α is increased, the results of v_{cr} for different γ are interesting. When the inclination angle α is relatively small, the stability of the pipe system is enhanced with increasing the gravity parameter γ. Nevertheless, when α is sufficiently large, the system stability may be weakened as γ is increased.

5   Nonlinear oscillation

To explore the global dynamical behaviors of the pipe system, the nonlinear oscillations of the soft pipe are discussed in this section.

Before doing some calculations, again, it is necessary to determine the suitable truncated-mode number N. The evolutions of oscillation amplitudes at $\xi = 1$ with increasing the dimensionless flow velocity are shown in Fig. 7. The good agreement between the results of $N = 3$ and $N = 4$ indicates that the calculations based on $N = 3$ are acceptable. Besides, each bifurcation diagram given in Fig. 7 shows that the system is stable when the flow velocity is below a critical value. Once the flow velocity is beyond the critical value, the pipe undergoes a limit cycle oscillation. This is in accord with the stability analysis results in Section 4. Moreover, the critical flow velocity obtained here quantitatively agrees well with the stability analysis results. In Fig. 7, it is also noted that the displacements of the pipe are relatively large, indicating that large-amplitude oscillations of the pipe occur.
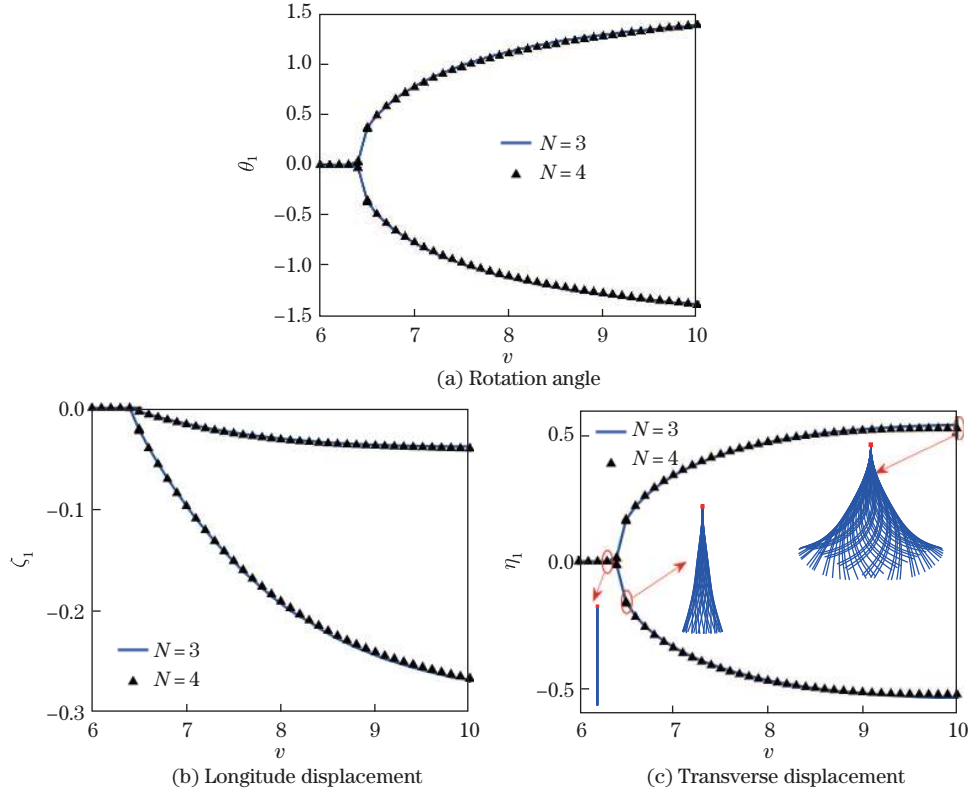
(a) Rotation angle

(b) Longitude displacement

(c) Transverse displacement

Fig. 7　Bifurcation diagrams for the tip-end responses of the pipe with $N = 3$ and $N = 4$ for $\alpha = 0$, $\beta = 0.142$, $\gamma = 18.9$, and $\mu = 5 \times 10^{-3}$. The deformed or oscillating shapes of the pipe in the global coordinate system for $v = 6.3$, 6.5, and 10 are added in (c) (color online)

　　To further study the effects of the gravity force on the nonlinear oscillation characteristics of the pipe, several bifurcation diagrams for different inclination angles are given in Fig. 8, where $\beta = 0.142$, $\gamma = 18.9$, and $\mu = 5 \times 10^{-3}$. As can be seen, when $\alpha = \pi$, as the flow velocity is increased from zero, the pipe would, in turns, undergo buckling instability, regain stability, and become unstable via flutter. These nonlinear results agree well with the stability analysis results shown in Section 4 from both qualitative and quantitative aspects. For the purpose of providing an easier-to-understand form of the results, the dynamic responses of the pipe are further represented in the global coordinate system. The free-end positions, including the coordinate of the vertical axis $X_{\mathrm{g}1}$ and the coordinate of horizontal axis $Z_{\mathrm{g}1}$, of the deformed (or oscillating) pipe are displayed in Figs. 9 and 10, where $\beta = 0.142$, $\gamma = 18.9$, and $\mu = 5 \times 10^{-3}$. In Fig. 9, the deformed or oscillating shapes of the pipe for several typical values of flow velocities $v = 6.4$, 6.5, 10, $v = 6.1$, 6.3, 10, $v = 5.3$, 5.5, 10, and $v = 2.0$, 4.1, 10 are added for Figs. 9(a), 9(b), 9(c), and 9(d), respectively. It can be observed that the dimensionless oscillation amplitude is close to 1, indicating that the pipe experiences extremely large-amplitude oscillations.

　　Combining Figs. 7–10, it is noted that all these nonlinear oscillations after flutter instability are period-1 motions.

　　The oscillating shapes of the pipe are worth discussing to further understand the nonlinear dynamical behaviors of the pipe system. The pipe shapes for typical flow velocity values are added in Figs. 7(c) and 9 for $\alpha = 0, \pi/4, \pi/2, 3\pi/4, \pi$. From Figs. 7(c), 9(a), 9(b), and 9(c), it can be found that the pipe has a static deformation when the flow velocity is below the critical value (v_{cr}), and will oscillate around the static deformation once the flow
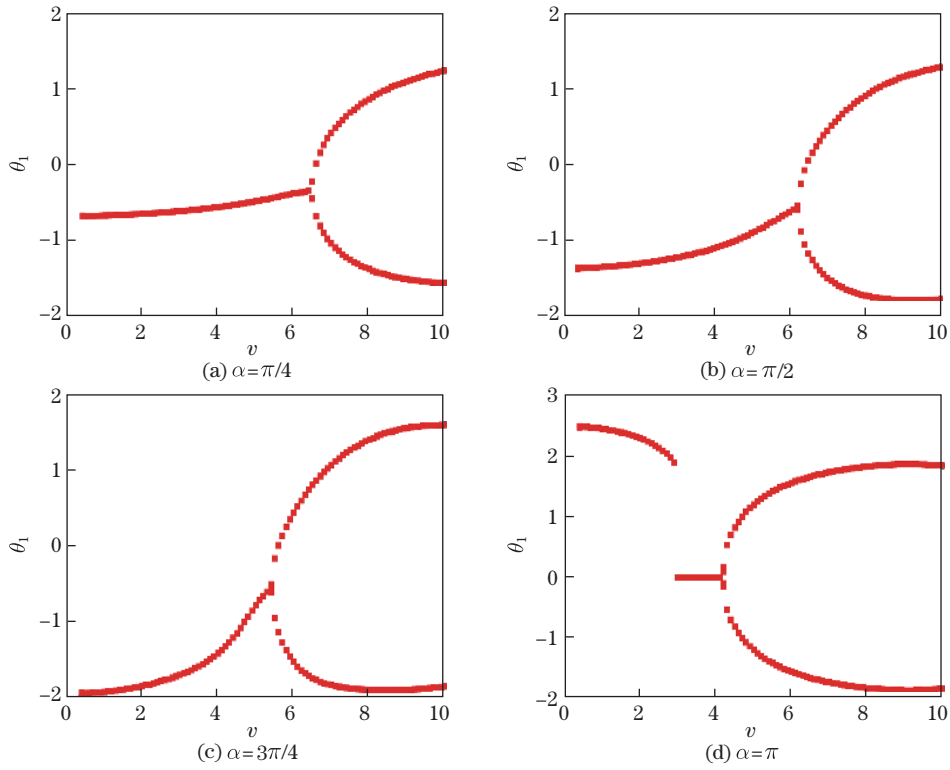
Fig. 8   Bifurcation diagrams for the rotation angle at the free end (color online)
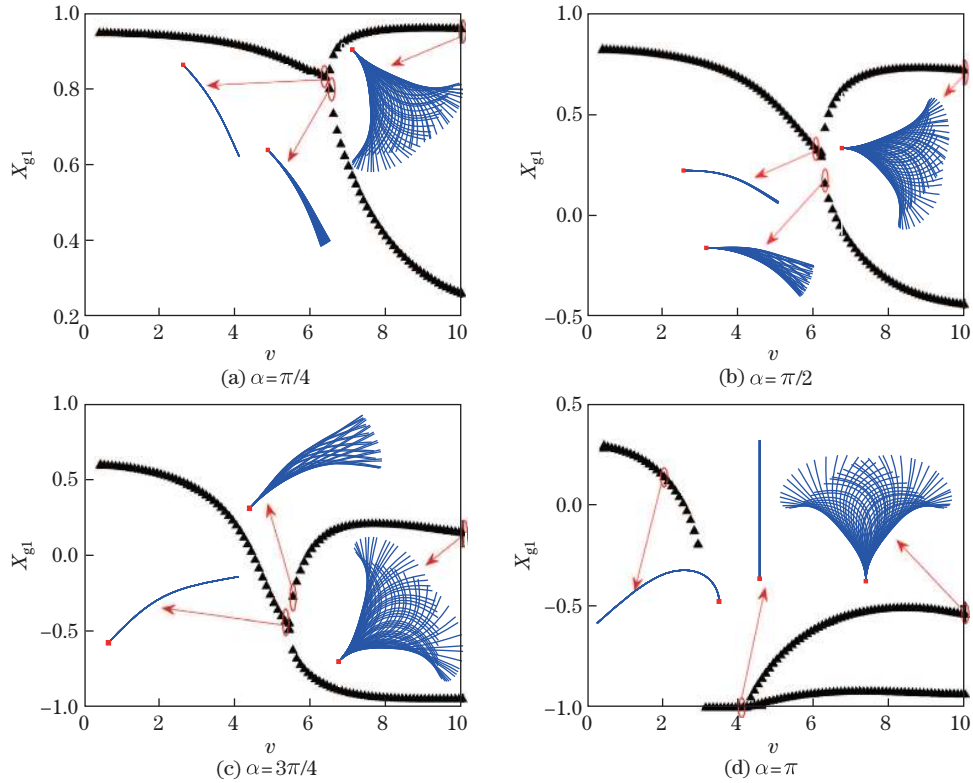
Fig. 9   Bifurcation diagrams for the vertical position of the tip-end in the global coordinate system (color online)
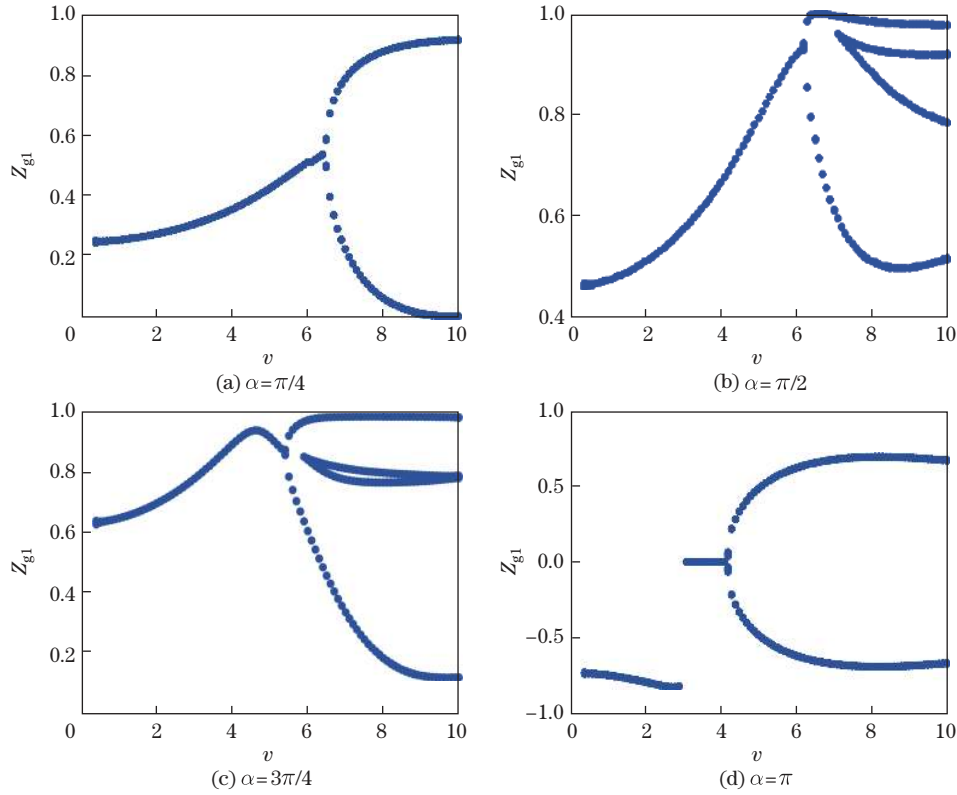
Fig. 10 Bifurcation diagrams for the horizontal position of the tip-end in the global coordinate system (color online)

velocity is beyond v_{cr}. Besides, a particular attention must be paid to the results of Fig. 9(d) for $\alpha = \pi$.

Time traces and phase trajectories are further called for the visual observations of the pipe's oscillations. Figure 11 shows the evolution of the coordinates of the tip-end position (X_{g1} and Z_{g1}) for the oscillating pipe with the variation of time, where $\beta = 0.142$, $\gamma = 18.9$, $\mu = 5 \times 10^{-3}$, and $v = 10$. The wide range of changes of the tip-end position shows that the pipe indeed undergoes extremely-large-amplitude oscillations. The phase trajectories for $v = 10$ and various inclination angles, including $\alpha = \pi/4$, $\pi/2$, $3\pi/4$, and π, are presented in Fig. 12, where $\beta = 0.142$, $\gamma = 18.9$, and $\mu = 5 \times 10^{-3}$. It is seen that the motions of the pipe are periodic.

Before leaving this section, the symmetry of the pipe system is discussed. When $\alpha = 0$ or π, the oscillation of the pipe is evidently symmetric. This symmetry feature can be easily understood by looking at the governing equation (20) and the results shown in Figs. 7(a), 7(c), 8(d), 9(d), and 10(d). As mentioned previously, buckling instability may occur for $\alpha = \pi$, providing that the flow velocity is relatively small and γ is sufficiently large. Due to the symmetry of the pipe system, the solution of the buckling configuration should have symmetric features and hence contain two symmetric branches. In this work, as shown in Figs. 8(d), 9(d), and 10(d), only one possible branch (left side) of the solutions has been plotted to distinguish the post-buckling and post-flutter behaviors in the bifurcation diagrams. The possible right-side branch of the solutions for all cases has not been graphically displayed. Besides, according to Eq. (20), it is also noted that the solution for a given value of α is antisymmetric with the solution for $\alpha - \pi$, since
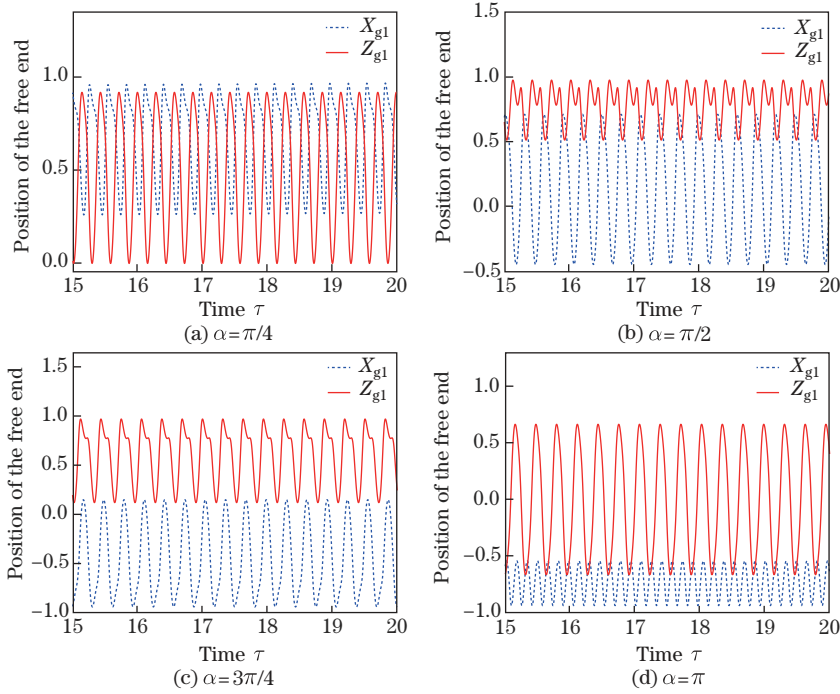
$$\sin(\theta + \alpha) = -\sin(\theta + \alpha - \pi).$$

Fig. 11 Time traces for the tip-end position of the pipe in the global coordinate system for various α (color online)
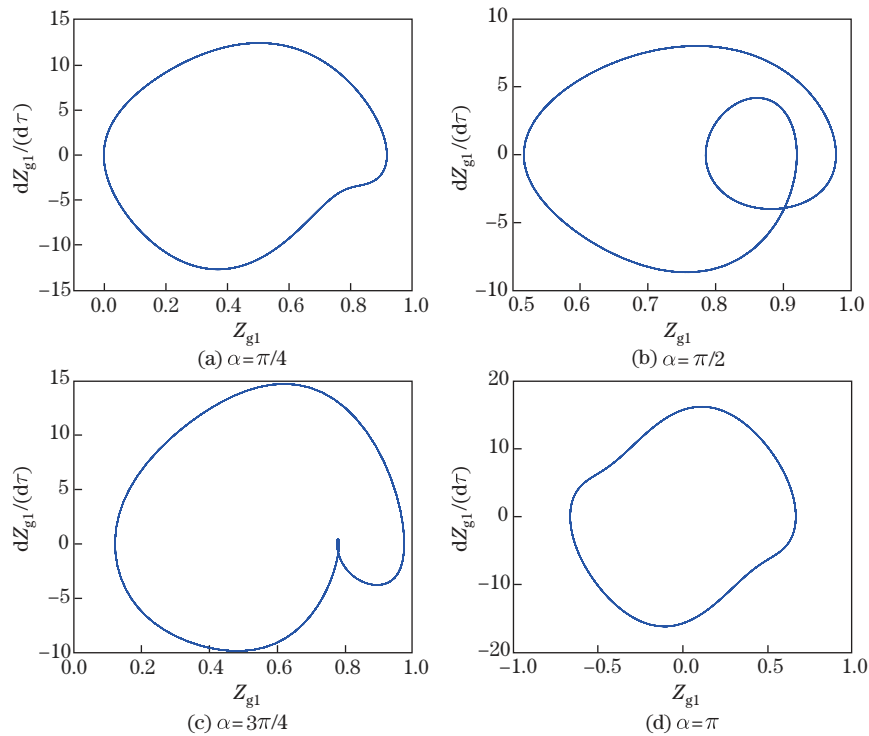

Fig. 12 Phase trajectories for the horizontal position of the tip end in the global coordinate system for various α (color online)

Accordingly, the analysis for the results in the range of $0 \leqslant \theta \leqslant \pi$ is enough to understand the large-amplitude oscillations of the soft pipe conveying fluid.

6   Conclusions

In this work, with particular attention to the gravity effect, the large-deformation static and dynamical behaviors of a cantilevered soft pipe conveying fluid are theoretically investigated. To describe the large-deformation responses of the soft pipe, the inclination angle between the undeformed pipe and the vertical line is introduced. Since the soft pipe is possibly subjected to extremely large deformations, the geometric nonlinearity due to the curvature effect is exactly taken into account without any approximation. Besides, both local and global coordinate systems are utilized for the purpose of deriving the governing equation. The derivation of the governing equation and the boundary conditions are based on the local coordinate system, and some of the numerical results are shown in the frame of the global coordinate system. The analyses of static deformations, stability, and nonlinear oscillations of the soft pipe are performed by considering the effects of several key parameters.

Both static and dynamic analyses show that the pipe would undergo extremely large deformations. The large-deformation behaviors of the soft pipe show some interesting features. The main conclusions of this work can be summarized as follows:

(i) The proposed theoretical model is able to predict the extremely large static deformations and dynamic oscillations of cantilevered soft pipes conveying fluid under the gravity force.

(ii) The static deformation of the pipe is strongly dependent on the inclination angle α and the gravity parameter γ but is hardly affected by the change of the mass ratio β.

(iii) Due to the static deformation, the stability of the pipe can be determined by analyzing the perturbation equation about the steady one. For $\alpha \neq \pi$, flutter is the preferred form of instability. In this case, the pipe's stability can be enhanced by increasing the mass ratio or gravity parameters and decreasing the inclination angle. For $\alpha = \pi$, however, the pipe successively undergoes buckling, stable, and flutter behaviors with increasing the flow velocity.

(iv) As the flow velocity is beyond the critical value, flutter of the pipe occurs around the static deformation position. When the flow velocity is sufficiently high, extremely large-amplitude oscillations can be produced in the form of limit-cycle motions.

In summary, gravity has a great effect on both static and dynamical behaviors of the soft pipe conveying fluid. The extremely large-amplitude oscillations of the soft pipe conveying fluid can be theoretically predicted by virtue of the geometrically exact model. The present study is expected to be helpful for designing and analyzing soft devices transporting fluid flows.

References

[1] WANG, Y. J., ZHANG, Q. C., WANG, W., and YANG, T. Z. In-plane dynamics of a fluid-conveying corrugated pipe supported at both ends. *Applied Mathematics and Mechanics* (*English Edition*), **40**(8), 1119–1134 (2019) https://doi.org/10.1007/s10483-019-2511-6

[2] JIANG, T. L., DAI, H. L., ZHOU, K., and WANG, L. Nonplanar post-buckling analysis of simply supported pipes conveying fluid with an axially sliding downstream end. *Applied Mathematics and Mechanics* (*English Edition*), **41**(1), 15–32 (2020) https://doi.org/10.1007/s10483-020-2557-9

[3] CHEN, W., DAI, H. L., and WANG, L. Enhanced stability of two-material panels in supersonic flow: optimization strategy and physical explanation. *AIAA Journal*, **57**, 5553–5565 (2019)

[4] PAÏDOUSSIS, M. P. *Fluid-Structure Interactions: Slender Structures and Axial Flow*, Academic Press, London, 63–75 (1998)

[5] BENJAMIN T. B. Dynamics of a system of articulated pipes conveying fluid, I: theory. *Proceedings of the Royal Society of London A*, **261**, 457–486 (1961)

[6] BENJAMIN, T. B. Dynamics of a system of articulated pipes conveying fluid, II: experiments. *Proceedings of the Royal Society of London A*, **261**, 487–499 (1961)

[7] GREGORY, R. W. and PAÏDOUSSIS, M. P. Unstable oscillation of tubular cantilevers conveying fluid, I: theory. *Proceedings of the Royal Society of London A*, **293**, 512–527 (1966)

[8] GREGORY, R. W. and PAÏDOUSSIS, M. P. Unstable oscillation of tubular cantilevers conveying fluid, II: experiments. *Proceedings of the Royal Society of London A*, **293**, 528–542 (1966)

[9] PAÏDOUSSIS, M. P. Dynamics of tubular cantilevers conveying fluid. *Journal of Engineering Mechanics*, **12**, 85–103 (1970)

[10] BOURRIÈRES, F. J. Sur un phénomène d'oscillation auto-entretenue en mécanique des fluides réels. *Publications Scientifiques et Techniques du Ministère de l'Air*, Centre de Documentation de l'Armement, Paris (1965)

[11] HOLMES, P. J. Pipes supported at both ends cannot flutter. *Journal of Applied Mechanics-Transactions of the ASME*, **45**, 619–622 (1978)

[12] HOLMES, P. J. Bifurcations to divergence and flutter in flow-induced oscillations: a finite-dimensional analysis. *Journal of Sound Vibration*, **53**, 471–503 (1977)

[13] WANG, L. H. and ZHONG, Z. Complex modal analysis for the time-variant dynamical problem of rotating pipe conveying fluid. *Computer Modeling in Engineering and Sciences*, **114**, 1–18 (2018)

[14] YANG, T. Z., JI, S. D., YANG, X. D., and FANG, B. Microfluid-induced nonlinear free vibration of microtubes. *International Journal of Engineering Science*, **76**, 47–55 (2014)

[15] TANG, Y. and YANG, T. Z. Post-buckling behavior and nonlinear vibration analysis of a fluid-conveying pipe composed of functionally graded material. *Composite Structures*, **185**, 393–400 (2018)

[16] SEMLER, C., LI, G. X., and PAÏDOUSSIS, M. P. The nonlinear equations of motion of pipes conveying fluid. *Journal of Sound Vibration*, **169**, 577–599 (1994)

[17] SARKAR, A. and PAÏDOUSSIS, M. P. A compact limit-cycle oscillation model of a cantilever conveying fluid. *Journal of Fluids and Structures*, **17**, 525–539 (2003)

[18] TANG, Y., YANG, T. Z., and FANG, B. Fractional dynamics of fluid-conveying pipes made of polymer-like materials. *Acta Mechanica Solida Sinica*, **31**, 243–258 (2018)

[19] LI, Q., LIU, W., LU, K., and YUE, Z. F. Nonlinear parametric vibration of a fluid-conveying pipe flexibly restrained at the ends. *Acta Mechanica Solida Sinica*, **33**, 327–346 (2020)

[20] PAÏDOUSSIS, M. P., SEMLER, C., WADHAM-GAGNON, M., and SAAID, S. Dynamics of cantilevered pipes conveying fluid, part 2: dynamics of the system with intermediate spring support. *Journal of Fluids and Structures*, **23**, 569–587 (2007)

[21] PAIDOUSSIS, M. P. and SEMLER, C. Nonlinear dynamics of a fluid-conveying cantilevered pipe with an intermediate spring support. *Journal of Fluids and Structures*, **7**, 269–298 (1993)

[22] GHAYESH, M. H., PAÏDOUSSIS, M. P., and MODARRES-SADEGHI, Y. Three-dimensional dynamics of a fluid-conveying cantilevered pipe fitted with an additional spring-support and an end-mass. *Journal of Sound Vibration*, **330**, 2869–2899 (2011)

[23] PAÏDOUSSIS, M. P. and SEMLER, C. Nonlinear and chaotic oscillations of a constrained cantilevered pipe conveying fluid: a full nonlinear analysis. *Nonlinear Dynamics*, **4**, 655–670 (1993)

[24] WANG, Y. K., WANG, L., NI, Q., DAI, H. L., YAN, H., and LUO, Y. Y. Non-planar responses of cantilevered pipes conveying fluid with intermediate motion constraints. *Nonlinear Dynamics*, **93**, 505–524 (2018)

[25] XU, Q. P. and LIU, J. Y. An improved dynamic model for a silicone material beam with large deformation. *Acta Mechanica Sinica*, **34**, 744–753 (2018)

[26] CHEN, W., WANG, L., and DAI, H. L. Nonlinear free vibration of hyperelastic beams based on Neo-Hookean model. *International Journal of Structural Stability and Dynamics*, **20**, 2050015 (2020)

[27] TEXIER, B. D. and DORBOLO, S. Deformations of an elastic pipe submitted to gravity and internal fluid flow. *Journal of Fluids and Structures*, **55**, 364–371 (2015)

[28] RIVERO-RODRIGUEZ, J. and PÉREZ-SABORID, M. Numerical investigation of the influence of gravity on flutter of cantilevered pipes conveying fluid. *Journal of Fluids and Structures*, **55**, 106–121 (2015)

[29] CHEN, W., DAI, H. L., JIA, Q. Q., and WANG, L. Geometrically exact equation of motion for large-amplitude oscillation of cantilevered pipe conveying fluid. *Nonlinear Dynamics*, **98**, 2097–2114 (2019)

[30] GHAYESH, M. H., PAÏDOUSSIS, M. P., and AMABILI, M. Nonlinear dynamics of cantilevered extensible pipes conveying fluid. *Journal of Sound Vibration,* **332**, 6405–6418 (2013)

[31] STOKER, J. J. *Nonlinear Elasticity*, Gordon and Breach, New York, 13–21 (1968)

[32] SNOWDON, J. C. *Vibration and Shock in Damped Mechanical System*, John Wiley, New York (1968)

[33] PAÏDOUSSIS, M. P. and SEMLER, C. Non-linear dynamics of a fluid-conveying cantilevered pipe with a small mass attached at the free end. *International Journal of Non-Linear Mechanics*, **33**, 15–32 (1998)